POLITECNICO DI TORINO
Repository ISTITUZIONALE

Electrochemical Behavior of Electron Beam Powder Bed Fused Ti536 Alloy under Simulated Inflammatory Conditions

Original
Electrochemical Behavior of Electron Beam Powder Bed Fused Ti536 Alloy under Simulated Inflammatory Conditions / Behjat, Amir; Sanaei, Saber; Mosallanejad, Mohammad Hossein; Atapour, Masoud; Saboori, Abdollah. - In: ACTA METALLURGICA SINICA. - ISSN 1006-7191. - 38:6(2025), pp. 969-980. [10.1007/s40195-025-01846-w]

Availability:
This version is available at: 11583/3001670 since: 2025-07-09T07:39:32Z

Publisher:
Springer

Published
DOI:10.1007/s40195-025-01846-w

Terms of use:

This article is made available under terms and conditions as specified in the corresponding bibliographic description in the repository

Publisher copyright

(Article begins on next page)

26 May 2026

Acta Metallurgica Sinica (English Letters)
https://doi.org/10.1007/s40195-025-01846-w

Electrochemical Behavior of Electron Beam Powder Bed Fused Ti536 Alloy under Simulated Inflammatory Conditions

Amir Behjat[1,2,3] · Saber Sanaei[3] · Mohammad Hossein Mosallanejad[1,2,3] · Masoud Atapour[3] · Abdollah Saboori[1,2]

Received: 2 November 2024 / Revised: 29 December 2024 / Accepted: 9 January 2025
© The Author(s) 2025

Abstract

Additive manufacturing (AM), as an advanced manufacturing technology, enables the production of personalized orthopedic implant devices with complex geometries that closely resemble bone structures. Titanium and its alloys are extensively employed in biomedical fields like orthopedics and dentistry, thanks to the excellent compatibility with the human body and high corrosion resistance due to the existence of a thin protective oxide layer known as TiO_2 upon exposure to oxygen on the surface. However, in joint inflammation, reactive oxygen species like hydrogen peroxide and radicals can damage the passive film on Ti implants, leading to their deterioration. Although AM technology for metallic implants is still developing, advancements in printing and new alloys are crucial for widespread use. This work aims to investigate the corrosion resistance of in-situ alloyed Ti536 (Ti5Al3V6Cu) alloy produced through electron beam powder bed fusion (EB-PBF) under simulated peri-implant inflammatory conditions. The corrosion resistance was evaluated using electrochemical experiments conducted in the presence of 0.1% H_2O_2 in a physiological saline solution (0.9% NaCl) to replicate the conditions that may occur during post-operative inflammation. The findings demonstrate that the micro-environment surrounding the implant during peri-implant inflammation is highly corrosive and can lead to the degradation of the TiO_2 passive layer. Physiological saline with H_2O_2 significantly increased biomaterial open circuit potential up to 0.36 mV vs. Ag/AgCl compared to physiological saline only. Potentiodynamic polarization (PDP) plots confirm this increase, as well. The PDP and electrochemical impedance spectroscopy (EIS) tests indicated that adding Cu does not impact the corrosion resistance of the Ti536 alloy initially under simulated inflammatory conditions, but prolonged immersion leads to enhanced corrosion resistance for all biomaterials tested, indicating the formation of an oxide layer after the reduction of the solution oxidizing power. These results suggest that modifying custom alloys by adding appropriate elements significantly enhances corrosion resistance, particularly in inflammatory conditions.

Keywords Additive manufacturing · Electron beam powder bed fusion · In-situ alloying · Electrochemical characterizations · Inflammatory conditions

1 Introduction

The increase in the elderly population in various countries has led to a rising demand for artificial implants. Over the years, metals and alloys have been used to implant in different areas of the human body, including the knee, hip, jaws, and spine, to enhance bodily functions and restore overall well-being and quality of life [1, 2]. Approximately, 80% of implant devices used in commercial settings consist of metallic biomaterials designed to address skeletal deformities. On the other hand, Ti and its alloys are commonly employed in biomedical applications, such as serving as a femoral stem in hip joint replacements and as screws in dental implants [3, 4]. However, titanium

Available online at http://link.springer.com/journal/40195

✉ Abdollah Saboori
abdollah.saboori@polito.it

[1] Department of Management and Production Engineering, Politecnico di Torino, Corso Duca degli Abruzzi 24, 10129 Turin, Italy

[2] Integrated Additive Manufacturing Center (IAM@PoliTo), Politecnico di Torino, Corso Castelfidardo 51, 10129 Turin, Italy

[3] Department of Materials Engineering, Isfahan University of Technology, Isfahan 84156-83111, Iran

Published online: 16 April 2025

processing can be challenging because of its high melting point, costly raw materials, poor thermal conduction, and intricate production procedures. The mentioned challenges can be resolved by the utilization of additive manufacturing (AM) techniques. AM, a developing technology known for its high flexibility and precise fabrication capabilities, among other capabilities, allows for the fabrication of multifunctional implants with complicated geometries that are difficult to produce otherwise [5, 6]. Metal AM encompasses several techniques, including powder bed fusion (PBF), directed energy deposition (DED), binder jetting, material extrusion, and sheet lamination [7, 8]. Each methodology presents unique benefits and is appropriate for various applications, such as aerospace, medical devices, and prototyping, depending on considerations such as the required material characteristics and the complexity of the components [9, 10]. PBF is a commonly utilized AM technique, with laser or electron beam PBF (L-PBF, EB-PBF) applied for selectively melting an already distributed powder bed. These methods are particularly effective for producing geometrically complex metallic implants [11].

Besides the processing aspects, the biocompatibility and corrosion resistance of the Ti alloys need to be evaluated for implant applications. The corrosion resistance of implant materials in various physiological solutions and their perceived biocompatibility are primarily attributed to the existence of a thin passive oxide layer on their surfaces [3, 4, 12]. Following the implantation of a biomaterial, the immune system of the body becomes activated in order to safeguard the host from infections and tissue harm [13, 14]. Due to the intricate in vivo setting and inflammatory mechanisms, the protective film on titanium implants begins to deteriorate, leading to accelerated degradation and corrosion of the implants. Indeed, inflammation triggers the generation of reactive oxygen species (ROS) like superoxide anions (O_2^-) and hydrogen peroxide (H_2O_2), which can significantly impair the corrosion resistance of titanium-based alloys [15]. Recent findings indicate that the corrosion of titanium alloys is heightened in the presence of hydrogen peroxide (H_2O_2) due to the formation of titanium ions such as Ti(IV)(+4 oxidation state) and H_2O_2 complex [16]. Moreover, hydrogen peroxide is a potent oxidizing agent in the oral cavity due to its synthesis by bacteria and involvement in inflammatory responses. As a result, the implant's mechanical behavior is impacted as the deterioration of the microstructure, for instance, through crack formation, can detrimentally influence key properties such as fatigue endurance limit. Consequently, this can substantially reduce the lifespan of the implants [16].

Despite the prominence of considering the presence of H_2O_2 when evaluating the behavior of metal implants, previous electrochemical research has primarily focused on testing in standard physiological saline and albumin solution, neglecting consideration of the peri-implant inflammatory environment [16–19]. On the other hand, recent studies suggest that incorporating suitable alloying additives into titanium alloys may serve as a viable approach to mitigate implant failures in inflammatory conditions. It has been shown that adding an appropriate amount of specific metals, such as niobium and zirconium, can enhance corrosion resistance, tribological performance, and biological compatibility [20, 21]. Copper is also frequently alloyed with Ti and its alloys to improve their antibacterial characteristics, resistance to corrosion, biocompatibility, and mechanical properties [22, 23], thanks to its significant solubility in β titanium, substantial atomic radius disparity compared to titanium, and the rapid precipitation of the Ti_2Cu phase from α-Ti [24].

Considering that AM methods can also be used to create new alloys by incorporating metallic elements into conventional alloys through in-situ alloying [25, 26], several reports have been conducted on adding Cu to Ti and its alloys using laser-assisted AM techniques to improve the performance of implants, as well as to enhance corrosion resistance and biological properties [27, 28]. Mosallanejad et al. [29] successfully produced Ti6Al4V–7Cu (Ti536) using EB-PBF and demonstrated the influence of employing an electron beam on the solidification behavior of the produced alloy during the AM process. Behjat et al. [23] investigated the same alloy in terms of bio-corrosion behavior in SBF solution, antibacterial features, and cell biocompatibility and introduced the alloy as a suitable candidate for load-bearing implants. However, despite the critical importance of evaluating the post-implantation behavior of the developed alloy, no literature data is reported on the Ti536 corrosion behavior in the H_2O_2 environment, with the existing corrosion assessments of AM Cu-bearing Ti alloys primarily carried out under standard conditions. As a result, limited data is available on their behavior in more complex environments relevant to post-implantation scenarios. Consequently, the primary aim of the current research is to conduct a comprehensive investigation into the corrosion characteristics of EB-PBF Ti536 alloy in the H_2O_2 environment. Additionally, the corrosion properties of Ti6Al4V were examined in the same solution to comparatively examine the interplay between Cu, as a solute in Ti alloys, and H_2O_2 solution.

2 Materials and Methods

2.1 Sample Fabrication

Extra-low interstitials (ELI) grade Ti6Al4V powders with spherical morphology (≤ 106 µm in size, averaging 75 µm, obtained from Arcam) and high purity Cu (≤ 2 µm in size,

6.6 µm, obtained from Sandvik Osprey Ltd.) powders were mixed in jar mill for 16 h to achieve a uniform Ti6Al4V-7Cu mixture. Arcam A2X EBM equipment was utilized to produce Ti6Al4V and Ti5Al3V6Cu cubic specimens using the standard parameters used for Ti6Al4V in the Arcam A2X system. Further details on the manufacturing procedure of the samples can be found in Ref. [29].

2.2 Microstructural Characterizations

The specimen's microstructures were investigated using an optical microscope (OM, Nikon EpipHot 300) and a scanning electron microscope (SEM, Philips XL, Netherlands) equipped with an energy-dispersive X-ray spectrometer (EDS) after standard metallographic preparations of samples, including grinding with silicon carbide paper to a grit size of #4000 and polishing with 1 and 0.3 µm diamond paste. The polished surfaces were first cleaned in an alcoholic ultrasonic bath for 10 min and then chemically etched with Kroll's reagent (HF: HNO_3: H_2O = 2:5:50) at room temperature for 2 min. To ensure accuracy, the EDS tests were performed in five different regions along the microscopy surface.

2.3 Corrosion Test

The corrosion behavior of Ti6Al4V and Ti5Al3V6Cu samples was studied using a PARSTAT 2273 and an AMETEK potentiostat/galvanostat with a conventional three-electrode cell system. A standard Ag/AgCl electrode in saturated potassium chloride was employed as a reference electrode, a platinum sheet served as the counter electrode, and the cold-mounted Ti6Al4V and Ti5Al3V6Cu samples were used as working electrodes. The surface area of the specimen exposed to the solution was 0.5 cm^2. The open circuit potential (OCP) was measured for 30 min, followed by electrochemical impedance spectroscopy (EIS) experiments conducted at the OCP. The EIS tests were performed in a frequency range from 100 kHz to 10 mHz and an alternating current (AC) amplitude of 10 mV. After the EIS analysis, a potentiodynamic polarization (PDP) scan was performed, ranging from − 250 to 1200 mVAg/AgCl versus OCP, with a scan rate of 1 mV/min, and the electrochemical assessments were conducted at 37 ± 2 °C in a water bath. Before conducting electrochemical measurements, the specimens underwent polishing up to #2400 grit. The corrosion assessments were carried out in a physiological saline solution (0.9% NaCl, 0.15 M) prepared by dissolving NaCl in deionized water. Moreover, a 33 mM (0.1%) H_2O_2 solution was added to the 0.9% NaCl solution to mimic an inflammatory condition. Each experiment was repeated at least twice to ensure reproducibility. Following PDP, the surfaces of both samples were examined using SEM under normal and inflammatory conditions.

3 Results and Discussion

3.1 Microstructures

The OM and SEM images of the samples across their building direction (BD) are illustrated in Fig. 1. As depicted in Fig. 1a, c, the Ti6Al4V alloy displays a characteristic acicular martensite structure in the cross section. The rapid cooling nature of the EB-PBF process resulted in a fine martensite structure. Conversely, the Ti5Al3V6Cu sample exhibited notable variations in microstructure morphology compared to the Ti6Al4V sample. This sample displayed a fully equiaxed microstructure with fine grains, as shown in Fig. 1b, along with narrow Ti_2Cu bands, as illustrated in Fig. 1d and referenced in a previous study [29].

Figure 2 shows the elemental distribution analysis obtained through EDS mapping for the Ti5Al3V6Cu microstructure to investigate the partitioning of elements between matrix phases and the Ti_2Cu secondary phase. The distribution of Cu within the matrix phase, specifically the alpha phase, is uniform, as depicted in Fig. 2, with no discernible regions enriched in Cu in this phase. This uniform distribution results from the large melt pool generated during the EB-PBF process, which promotes the melting of Cu powders and enhances the mixing of the resulting melt with molten Ti. Typically, the formation of Ti_2Cu precipitates may occur through eutectoid decomposition of the beta phase or precipitation from the supersaturated alpha phase, a phenomenon attributed to the reduced solubility of Cu in the alpha phase at lower temperatures [29].

3.2 Corrosion Studies

3.2.1 Open Circuit Potential (OCP)

Figure 3 presents the OCP variations of Ti6Al4V and Ti5Al3V6Cu specimens following immersion in simulated media for 2 and 24 h. Analysis of the OCP graph indicates that adding 0.1% H_2O_2 to a 0.9% NaCl solution notably shifted the potential toward a positive direction, while the OCP in 0.9% NaCl solution displayed a more negative potential. The observed rise in positive potential in the presence of H_2O_2 can be ascribed to the decomposition of H_2O_2 into H_2 and O_2. This decomposition serves as an additional cathodic reaction to the reduction of oxygen. Previous research has suggested that the positive

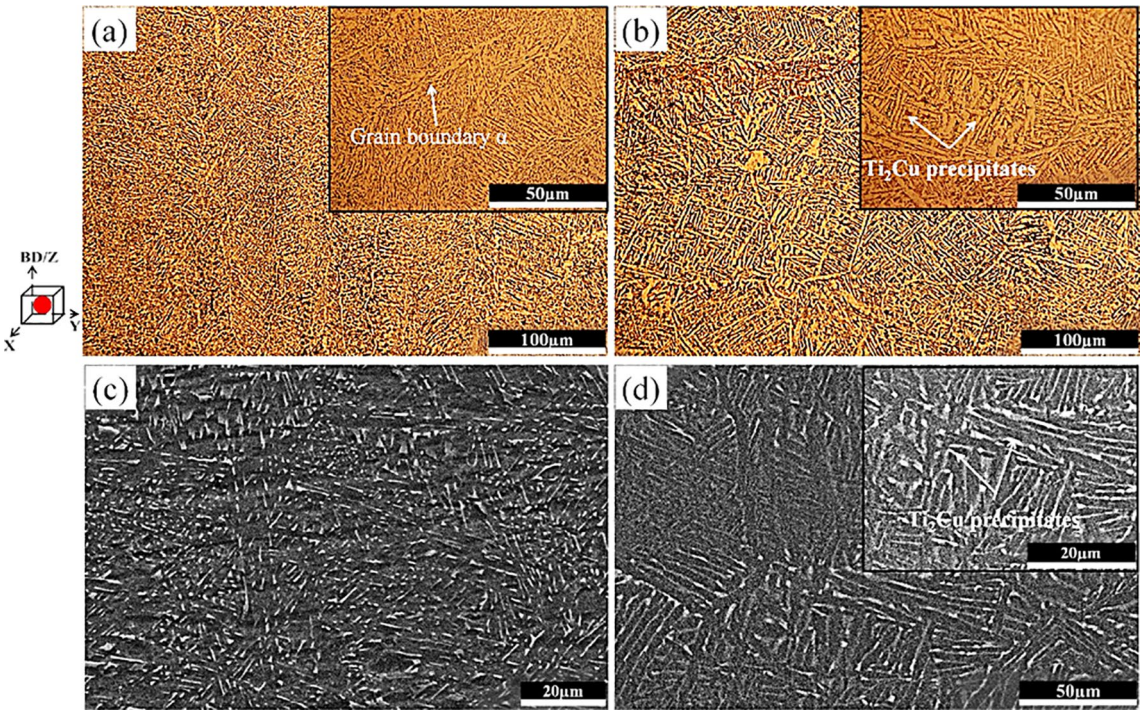

Fig. 1 OM and SEM of **a**, **c** Ti6Al4V and **b**, **d** Ti5Al3V6Cu samples.

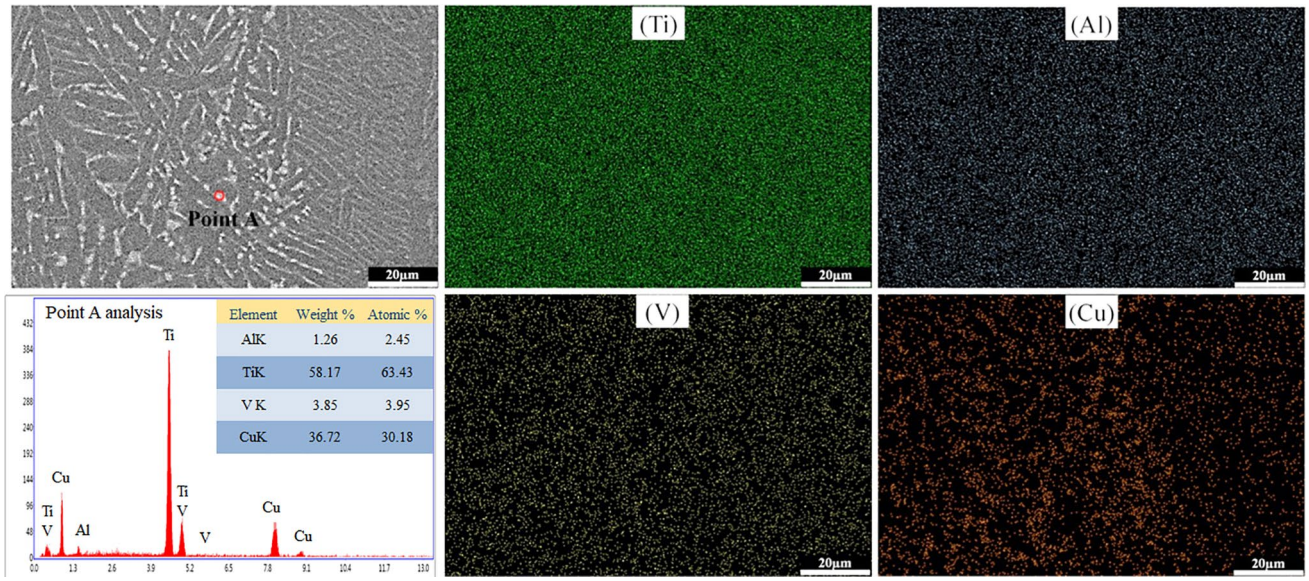

Fig. 2 EDS mapping of Ti5Al3V6Cu sample.

OCP in H_2O_2-containing solutions is often induced by intermediates with strong oxidizing properties, such as H_2O and OH, which adsorb on the Ti-based biomaterials

passive film [30, 31]. Additionally, the OCP values increased over time, indicating the formation of an oxide layer, thicker than the native TiO_2 film, on the sample surface.

3.2.2 Potentiodynamic Polarization

Figure 4 depicts polarization resistance curves obtained following a 2 h immersion in both normal and inflammatory environments for the two samples.

It is evident that under normal circumstances, both samples exhibit passivation characteristics in the anodic region. The anodic current density remains relatively

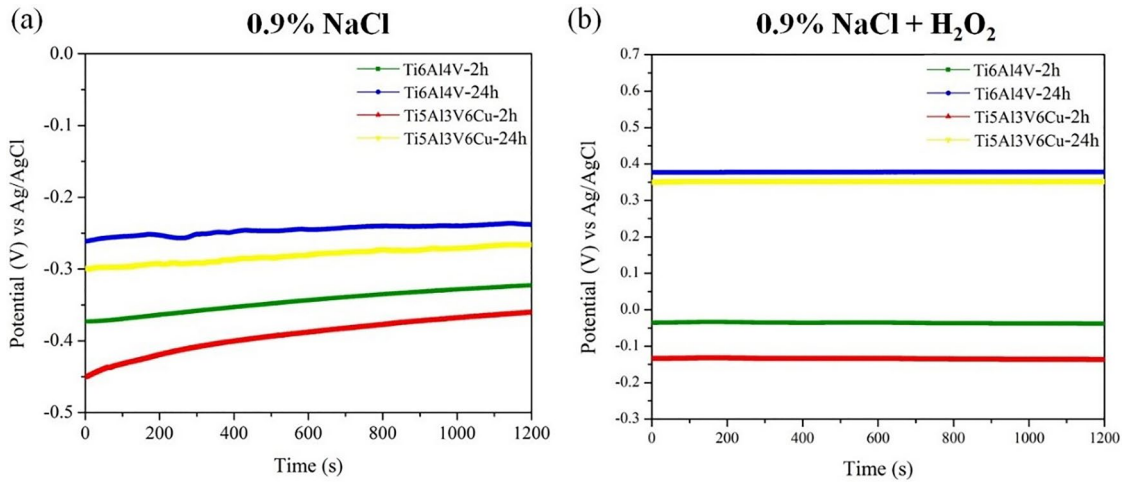

Fig. 3 OCP curves recorded for samples after 2 h and 24 h of immersion in **a** 0.9% NaCl, **b** 0.9% NaCl+H_2O_2.

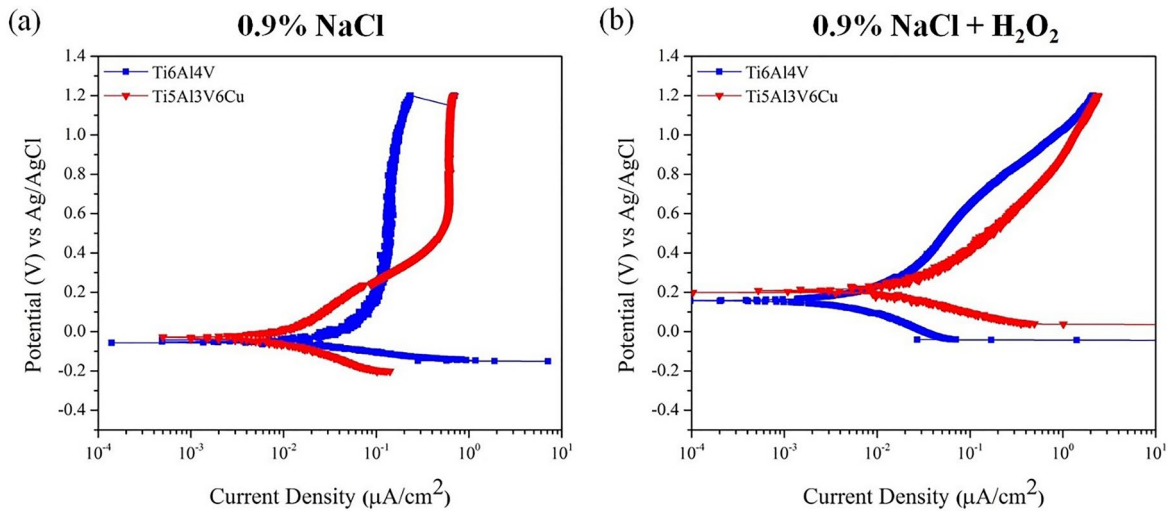

Fig. 4 PDP curves recorded for samples after 2 h of immersion in **a** 0.9% NaCl, **b** 0.9% NaCl+H_2O_2.

Table 1 Electrochemical parameters of the samples in different simulated conditions

Simulated conditions	Samples	E_{corr} (V vs. Ag/AgCl)	I_{corr} (μA·cm^{-2})	I_{pass} (μA·cm^{-2})
0.9% NaCl	Ti6Al4V	− 0.025 ± 0.138	0.042 ± 0.004	0.39 ± 0.03
	Ti5Al3V6Cu	− 0.035 ± 0.015	0.026 ± 0.002	6.17 ± 0.06
0.9% NaCl + H_2O_2	Ti6Al4V	0.165 ± 0.013	0.031 ± 0.003	–
	Ti5Al3V6Cu	0.203 ± 0.174	0.044 ± 0.004	–

constant across the potential range (up to 1200 mV vs. Ag/AgCl) without any potential breakdown, indicating the stable formation of the oxide layer. Conversely, in the presence of H_2O_2 in the inflammatory solutions, the specimens do not demonstrate passive behavior, and the anodic current density (above 300 mV vs. Ag/AgCl) shows an increasing trend with rising anodic polarization. Despite the elevated anodic current density, no signs of potential breakdown were observed due to H_2O_2.

The corrosion performance of samples was assessed through the measurement of corrosion potential (E_{corr}), corrosion current density (I_{corr}), and passive current density (I_{pass}). The values of E_{corr}, I_{corr}, and I_{pass} were obtained using the Tafel extrapolation technique and are presented in Table 1.

As shown in Table 1, the I_{corr} of Ti5Al3V6Cu specimen has been observed to increase compared to Ti6Al4V. This reduction in I_{corr} in normal media may be attributed to the development of a stable surface oxide film that acts as a protective barrier against further corrosion. Adding H_2O_2 into the 0.9% NaCl solution changed the corrosion mechanism from passivation behavior in anodic branches into active behavior. Indeed, an increase in I_{corr} values for both samples indicates a higher corrosion rate under inflammatory conditions, as depicted in Fig. 3a, b. These findings align with prior research demonstrating elevated I_{corr} of Ti6Al4V in biological solutions containing H_2O_2 [16, 32]. Furthermore, under inflammatory conditions, the I_{corr} values for the Ti5Al3V6Cu specimen gradually increased oxidation of the metal surface when exposed to H_2O_2-containing solutions. However, the oxide layer formed dissolves faster than required for optimal protection. Consistent with the OCP illustrated in Fig. 2b, the corrosion potential (E_{corr}) values were more electropositive in the inflammatory environment (H_2O_2-containing 0.9% NaCl) compared to the normal conditions.

3.2.3 Electrochemical Impedance Spectroscopy

Figure 5 illustrates the Nyquist and Bode phase plots derived from EIS experiments. The obtained data reveals that the impedance value of Ti6Al4V surpasses that of Ti5Al3V6Cu, suggesting that the passivation film of Ti6Al4V exhibits superior corrosion resistance in 0.9% NaCl solution compared to Ti5Al3V6Cu. Furthermore, it is worth noting that based on the Nyquist plots, a passive film with a larger loop radius for the Ti6Al4V sample suggests increased impedance, indicating the challenge of electron transfer between the sample and the electrolyte [30]. It is also evident from Fig. 5a that the diameter of capacitive semicircles decreases upon adding H_2O_2 to 0.9% NaCl for both samples, signifying a deterioration in corrosion resistance under inflammatory conditions. This observed corrosion behavior aligns with findings from previous investigations involving H_2O_2-containing biological solutions [16, 31, 33].

Figure 5b depicts the Bode phase plots corresponding to Ti6Al4V and Ti5Al3V6Cu alloys, respectively. Under normal conditions, the impedance remained stable with a phase angle approaching 0°, indicative of the electrolyte resistance. The introduction of H_2O_2 into the electrolyte resulted in a reduction in corrosion resistance during the initial immersion stage. This decline was attributed to the erosion of the passive film by 0.9% NaCl, leading to the formation of a more defective passive layer that facilitated the dissolution of Ti. Furthermore, both alloys subjected to the corrosive environment for 24 h exhibited phase angles near 80°, confirming their exceptional corrosion resistance and reduced reactivity. This suggests that adding Cu has a minimal impact on the corrosion properties of Ti6Al4V after a 24 h exposure by forming a more stable passive layer.

The EIS findings were assessed using the equivalent circuit (ECC) model to fit the passive layer. Within the ECC (depicted in the inset of Fig. 5a), distinct components symbolize R_s and R_p, which stand for the solution resistance and resistance of the oxide film, respectively, while CPE represents the constant phase element. The electrochemical parameters derived from the impedance data analysis software are detailed in Table 1. The presence of CPE signifies a departure from ideal capacitance due to the formation of non-capacitive passive films resulting from a multifaceted corrosion mechanism. Various irregularities, such as surface roughness, impurities, or imperfections, necessitated the introduction of a CPE component instead of a simple capacitor [34, 35]. The impedance of the CPE is defined as per the following equation:

$$Z_{CPE} = Y_0(\omega^n j)^{-1}. \tag{1}$$

where Y_0 is a frequency-independent constant, ω is the angular frequency, n ($0 \le n \le 1$) is the phase constant exponent, and j is the imaginary unit ($j^2 = -1$). If n is equal to 0, the CPE is resistive, whereas if it is equal to 1, the CPE is capacitive. The Brug model was utilized to determine the effective capacity (C_{eff}) of each passive layer [36]:

$$C_{eff} = \sqrt[n]{Q \cdot R_T^{1-n}}. \tag{2}$$

where the total resistance (R_T) is the sum of R_s and R_p. The capacitance can be related to the thickness of the film (L_{SS}) using the following equation:

$$L_{ss} = \frac{\varepsilon\varepsilon 0A}{C_{eff}}. \tag{3}$$

where the ε denotes the relative permittivity of the material, which is commonly found to be approximately 45 for the passive film of TiO_2 [30, 37]. The symbol ε_0 refers to

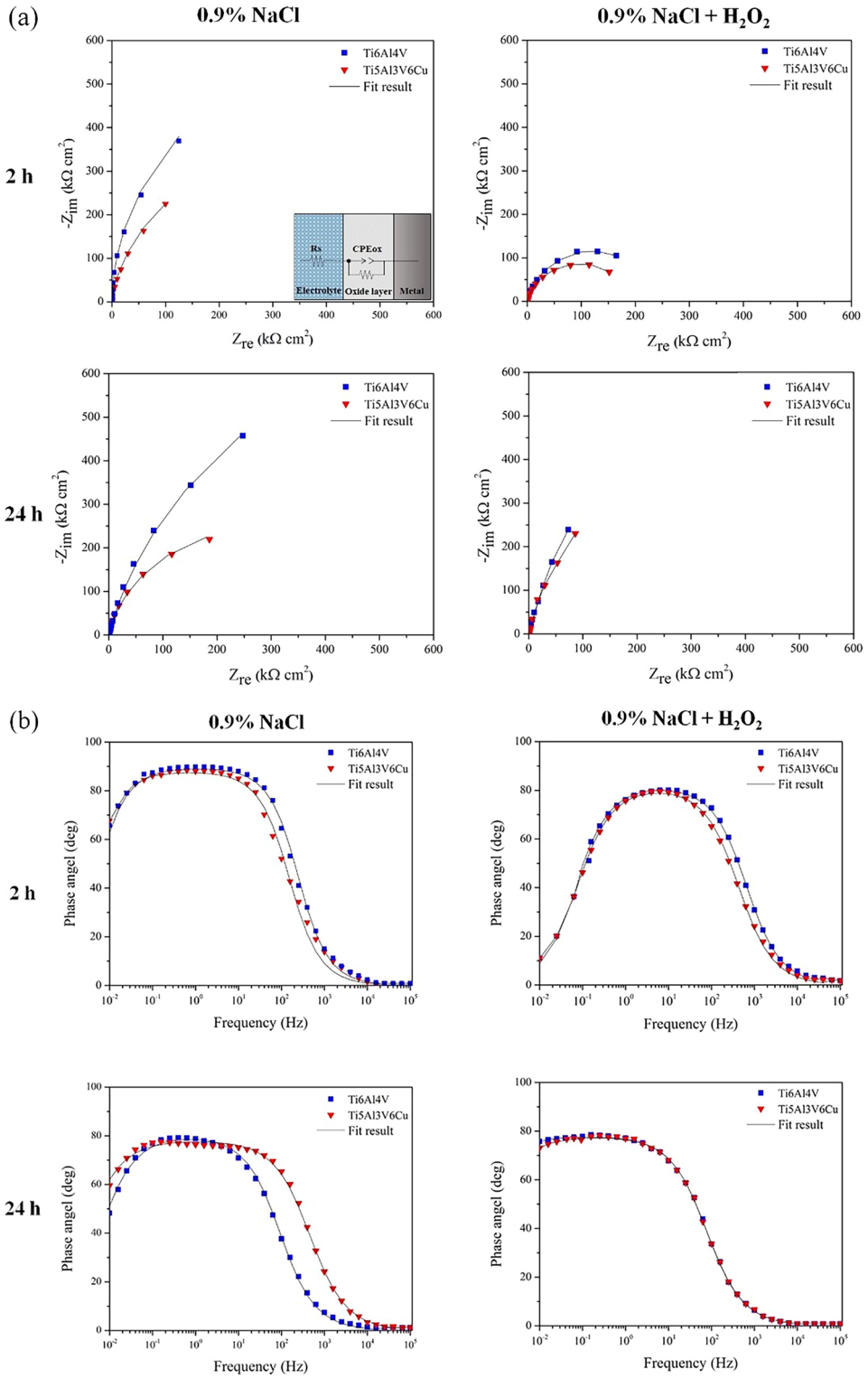

Fig. 5 **a** Nyquist plots, and **b** Bode phase plots for the samples.

the permittivity of vacuum, which is approximately 8.854×10^{-14} F cm^{-1}, and A represents the surface area.

Based on the findings presented in Table 2, it is observed that the resistances of passive layers, as indicated by the R_p

Table 2 Parameters determined from fitting the EIS plots of the samples in different simulated conditions

Simulated conditions	Immersion time (h)	Samples	R_s (Ω cm^2)	R_p (kΩ cm^2)	Q_{pl} (10^{-5} Ω^{-1} cm^{-2} S^n)	n	C_{eff} (10^{-5} F cm^{-2})	d_{eff} (nm)
0.9% NaCl	2	Ti6Al4V	73.73 ± 0.13	44.53 ± 0.23	6.42 ± 0.23	0.87	2.93 ± 0.13	1.36 ± 0.17
		Ti5Al3V6Cu	73.62 ± 0.12	19.94 ± 0.16	6.41 ± 0.08	0.86	2.48 ± 0.12	1.61 ± 0.14
	24	Ti6Al4V	57.27 ± 0.12	53.18 ± 0.13	6.82 ± 0.15	0.88	2.834 ± 0.23	1.41 ± 0.16
		Ti5Al3V6Cu	59.61 ± 0.15	25.6 ± 0.12	7.08 ± 0.14	0.87	2.12 ± 0.16	1.88 ± 0.12
0.9% NaCl + H_2O_2	2	Ti6Al4V	97.31 ± 0.22	5.88 ± 0.14	3.21 ± 0.15	0.89	1.65 ± 0.07	2.04 ± 0.11
		Ti5Al3V6Cu	83.99 ± 0.81	2.03 ± 0.31	1.96 ± 0.08	0.89	1.52 ± 0.05	2.13 ± 0.13
	24	Ti6Al4V	68.09 ± 0.23	17.76 ± 0.53	1.76 ± 0.29	0.90	1.93 ± 0.13	2.64 ± 0.21
		Ti5Al3V6Cu	51.30 ± 0.15	12.3 ± 0.14	1.93 ± 0.14	0.87	1.87 ± 0.13	2.46 ± 0.14

values, are adversely affected by inflammatory conditions, leading to a reduction in their resistance. This phenomenon can be attributed to the creation of Ti(IV)-H_2O_2 complex compounds resulting from the interaction between titanium and H_2O, which exhibit limited resistance against corrosive substances. The R_p values for all samples showed an increase after 24 h in all solutions, indicating the development and enhancement of a protective passive film. In environments with inflammation, the concentration of H_2O_2 decreases over time due to its decomposition into H_2O and O_2, thereby reducing the oxidative potential of the medium and promoting the self-repair of the passive layer [16].

The determined passive layer thickness values were found to be within a few nanometers, a range consistent with findings from previous reports ref. This reduced compactness of the passive film is correlated with the elevated CPE values. The significantly higher CPE values observed in the corrosive environment suggest a decline in corrosion resistance. Exposure of a specimen to H_2O_2 results in damage to the passive film, leading to increased surface dissolution and acceleration of the cathodic reaction rate. Moreover, all samples exhibited an increase in R_p after 24 h under all test conditions, indicating the formation and growth of a protective passive film that aids in the self-repair of passive layers in corrosive media and the impact of H_2O_2 decomposition into H_2O and O_2.

3.2.4 Surface Morphology after PDP Tests

The surfaces of the samples were examined using SEM following a 2 h immersion period, during which the corresponding PDP curves were recorded in each simulated solution. Distinct variations in surface morphologies were observed between the Ti6Al4V and Ti5Al3V6Cu specimens under normal and inflammatory conditions. As depicted in Fig. 6a, c, a limited number of pits were observed, along with the presence of general corrosion characterized by the formation of a gray-colored passive film on the surfaces of both samples in the normal environment.

Figure 6b, d illustrates the irregular structure and multiple pits containing corrosion by-products that were generated by adding H_2O_2 into the solution, indicating the disintegration of samples in the presence of H_2O_2 and Cl ions. Similar structural features have been documented for Ti6Al4V under inflammatory circumstances in prior studies, which highlighted the direct impact of H_2O_2 on the characteristics of the surface layer developed on Ti alloys [16]. In inflammatory environments, the adsorption of Cl^- ions to oxygen vacancy sites on the surface of the oxide/solution in the presence of H_2O_2 triggers a movement of cation vacancies toward the metal oxide interface. The accumulation of excess cation vacancies promotes the initiation of pit formation.

Based on the above results, the presence of copper within titanium alloys can significantly impact their corrosion behavior when exposed to H_2O_2. Copper-enriched areas can serve as cathodic sites, thereby facilitating localized or galvanic corrosion when in contact with titanium [38]. Galvanic corrosion is one of the most prevalent forms of corrosion affecting alloys in electrolyte solutions, typically arising from the creation of micro-galvanic couples due to potential differences between the anode and cathode phases [39]. It has been reported that there are differences in surface potential between the α, β, and Ti_2Cu phases, with the surface potential ranked as follows: $\alpha \gg Ti_2Cu > \beta$ [40]. Consequently, it can be concluded that the electrochemical reactions cause micro-cathodes to accelerate the dissolution of the micro-anodes, particularly by disrupting the spontaneous oxide film formed on the sample surface. Several parameters, such as thermal cycle, component size, and chemical composition, could affect the phase fraction of titanium alloys and change the corrosion properties [19, 41, 42]. In a typical corrosive environment, the presence of these heterogeneous phases can enhance the micro-galvanic effect, leading to increased dissolution rates of

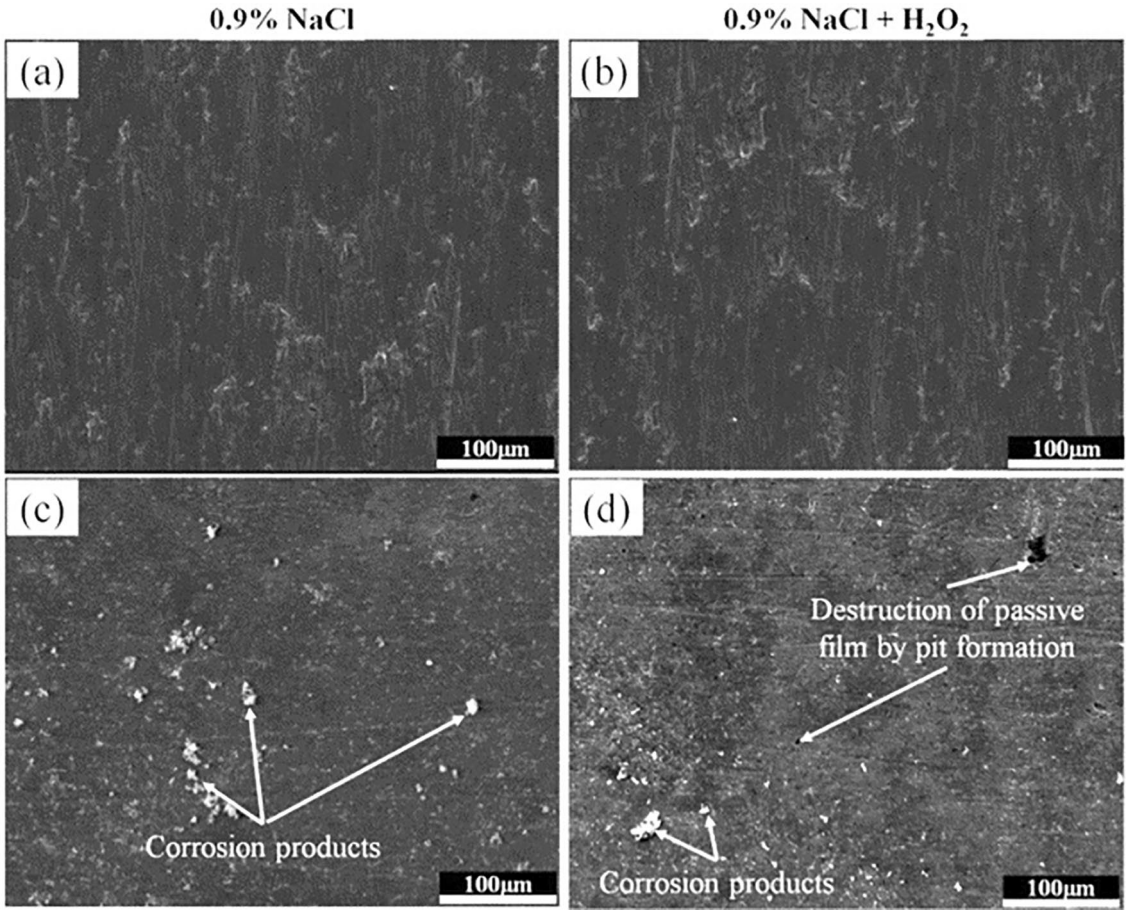

Fig. 6 SEM of samples after PDP test in **a**, **b** Ti6Al4V, **c**, **d** Ti5Al3V6Cu.

Ti6Al4V and Ti5Al3V6Cu alloys. However, the formation of a spontaneous passivation film, such as TiO_2, significantly inhibits the progression of corrosion. Adding H_2O_2 can exacerbate the corrosive effects on the Ti alloy due to redox reactions involving Cu, H_2O_2, and other chemical species within the solution. Moreover, the interaction between Cu within the sample and H_2O_2 solutions can develop intricate surface layers or films comprising Cu compounds, titanium oxides, and various reaction by-products. These film compositions and characteristics play a crucial role in determining the titanium alloy's corrosion resistance and surface properties. Notably, the observed increase in the corrosion current density (I_{corr}) under inflammatory conditions for Ti5Al3V6Cu (Fig. 4) is attributed to the presence of copper oxide on the Ti6Al4V alloy surface, leading to the formation of vacancies within the oxide layers, a process further accelerated by the presence of hydrogen peroxide and chloride ions [43].

A schematic illustrating the corrosion mechanism and various phenomena occurring on the surfaces of Ti6Al4V and Ti5Al3V6Cu alloys when exposed to normal and inflammatory environments is presented in Fig. 7.

It is important to note that the dissolution rate of the metal, in cases where the passive film is damaged, is generally linked to the resistance of the passive film. Based on the EIS data, the passive film resistance of Ti6Al4V is marginally higher than that of Ti5Al3V6Cu during both immersion periods. Furthermore, after 24 h, an increase in passive film resistance is observed, indicating the formation and growth of a passive protective film.

The influence of H_2O_2 on titanium oxide formation is explained through the following reactions (4–6):

$$2H_2O_2 \rightarrow 2H_2O + O_2. \quad (4)$$

With the following intermediate steps:

$$2TiO_2 + H_2O_2 + e^- \rightarrow Ti_2O_3 + H_2O + O_2. \quad (5)$$

$$Ti_2O_3 + H_2O_2 \rightarrow 2TiO_2 + H_2O + 2e^-. \quad (6)$$

As depicted in Fig. 7, the surface layer of the alloy exhibits a higher concentration of metallic ions in the 0.9% NaCl + H_2O_2 solution compared to the NaCl-only solution. This enhancement is attributed to H_2O_2 acting as an oxidizing

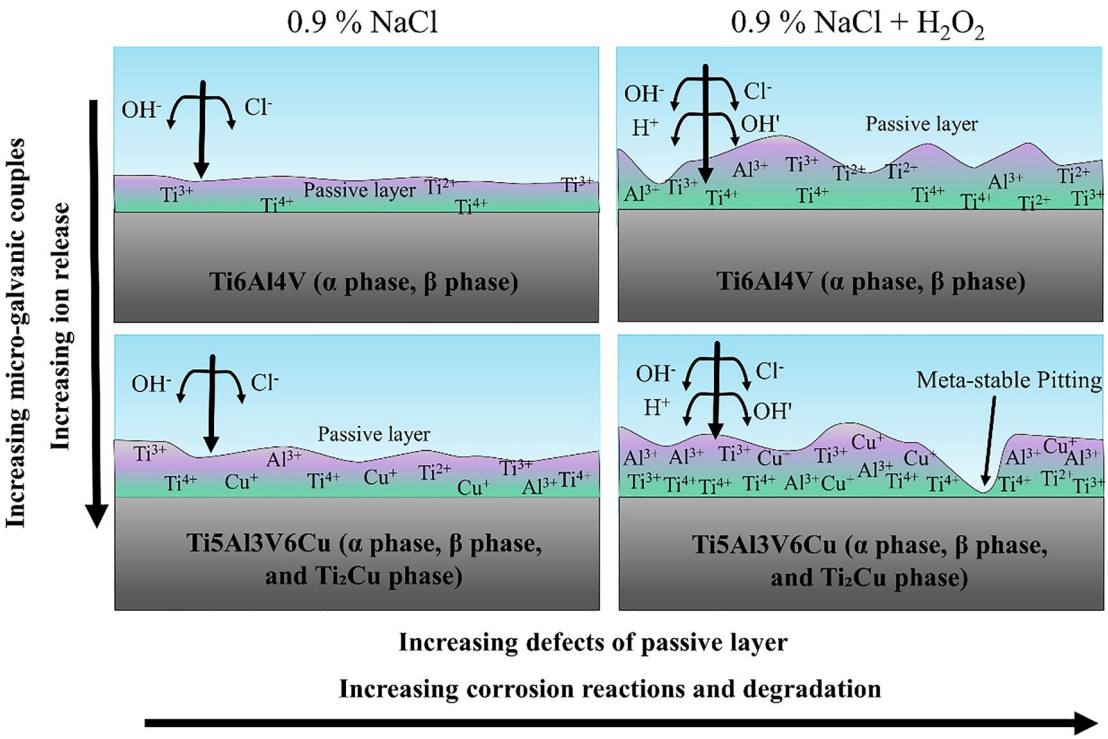

Fig. 7 Schematic representation of the corrosion mechanism on Ti6Al4V and Ti5Al3V6Cu alloy surfaces present in the normal and inflammatory tested environments.

agent, facilitating the formation of either a TiOOH defective complex or an H_2O_2–TiO_2 complex [44]. These complexes contribute to the generation of oxygen vacancy sites on the oxide/solution interface, thereby accelerating the release of metal ions [32, 45, 46]. Previous studies examining the passivation behavior of Ti6Al4V in lactic acid-containing environments have demonstrated that the formation of oxygen vacancies is enhanced, accompanied by a reduction in the thickness of the passive film [16, 20, 47]. This reduction is associated with the suppressed conversion of Ti^{3+} and Ti^{2+} to Ti^{4+} on the material's surface.

From the perspective of the influence of copper, it could be said that copper ions are released from the alloy surface through redox reactions (4-8), which initiate a series of subsequent chemical processes.

$$Cu^{2+} + 2OH^{-} \rightarrow Cu_2O + 2H_2O. \quad (7)$$

$$Cu^{+} + O_2 + 2H^{+} \rightarrow Cu^{2+} + H_2O_2. \quad (8)$$

Also, when hydrogen peroxide is present, the interaction between oxygen and transition metal ions like copper can lead to the generation of hydroxyl radicals (OH′), which in turn enhances the reactivity of the electrolyte toward the titanium alloy surface, as illustrated below:

$$Ti^{3+} + H_2O_2 \rightarrow Ti^{4+} + OH^{-} + OH'. \quad (9)$$

$$Cu^{+} + H_2O_2 \rightarrow Cu^{2+} + OH^{-} + OH'. \quad (10)$$

These reactions near the surface destabilizing the oxide film [16].

Additionally, it has been observed that incorporating alloying elements with higher valence electrons, such as niobium (Nb^{5+}) or tantalum (Ta^{5+}), can help compensate for the reduced positive charge in the titanium oxide layer caused by the presence of Ti^{3+} and Ti^{2+} ions. This modification leads to a decrease in the number of oxygen vacancies within the passive film, enhancing its stability and improving the corrosion resistance [31, 42, 48, 49]. However, for Ti5Al3V6Cu alloy, Cu ions, which have a lower valence than Ti, can increase the donor density in the film, thereby boosting its conductivity [23]. It is believed that this higher donor concentration results from copper atoms occupying interstitial sites $\left(Cu_i^{+}\right)$ in the defective titanium oxide lattice, potentially acting as electron donors. These Cu cation species are more mobile than Ti cations due to the cation vacancy mechanism, resulting in a considerable portion of the current being conducted by Cu interstitials in a short immersion time [50]. However, it is important to highlight that forming a thick passive film and corrosion products on the surface after 24 h of

immersion reduces the release of Cu ions, thereby enhancing the corrosion resistance of the Ti5Al3V6Cu alloy. In other words, the initial protection provided by the thin, dense TiO_2 passive layer is gradually replaced by a thicker, more porous titanium oxide coating with improved barrier properties. This phenomenon has been explained by previous studies, which suggest that, after immersion, Cu substitution in the passive film strengthens the electrostatic interaction between the immobilized Cu cation sublattice ($Cu_{Ti}^{X'}$) within the Ti lattice and the mobile cation interstitials (Cu_i^+). This interaction forms complexes that reduce the flux of Cu interstitials through the barrier layer (passive film), which in turn lowers the passive current density and corrosion rate [40, 50].

4 Conclusions

In summary, this research highlights the electrochemical degradation of an innovative Cu-bearing titanium fabricated using EB-PBF. The electrochemical assessments investigated the impact of immersion duration and simulated biological environments on the corrosion behavior of Ti6Al4V and Ti5Al3V6Cu biomaterials. The ensuing final remarks can be highlighted as follows:

1. The OCP monitoring data demonstrates a trend toward more positive values over time, attributed to an increase in the thickness of the passive layer under normal conditions and the decomposition of H_2O_2 over time during inflammatory conditions.
2. The PDP results indicate an increase in I_{corr} values for both samples in inflammatory conditions, suggesting the role of H_2O_2 in passive layer degradation. The presence of H_2O_2 in the inflammatory environment prevented specimens from exhibiting passive behavior.
3. EIS analysis reveals that the addition of H_2O_2 to saline solution diminishes the corrosion resistance of both alloys.
4. Adding Cu initially does not impact the corrosion resistance of titanium alloy in simulated inflammatory conditions, but prolonged immersion leads to enhanced corrosion resistance for all the samples tested, indicating the formation of an oxide layer after the reduction of the solution's oxidizing power.
5. SEM micrographs illustrate alterations in the surface morphology of Ti alloys when exposed to solutions containing H_2O_2, resulting in the dissolution of the titanium oxide passive film and increased susceptibility to corrosion.

Funding Open access funding provided by Politecnico di Torino within the CRUI-CARE Agreement.

Declaration

Conflict of interest The authors state that there are no conflicts of interest to disclose.

Open Access This article is licensed under a Creative Commons Attribution 4.0 International License, which permits use, sharing, adaptation, distribution and reproduction in any medium or format, as long as you give appropriate credit to the original author(s) and the source, provide a link to the Creative Commons licence, and indicate if changes were made. The images or other third party material in this article are included in the article's Creative Commons licence, unless indicated otherwise in a credit line to the material. If material is not included in the article's Creative Commons licence and your intended use is not permitted by statutory regulation or exceeds the permitted use, you will need to obtain permission directly from the copyright holder. To view a copy of this licence, visit http://creativecommons.org/licenses/by/4.0/.

References

[1] D.E. Reichman, J.A. Greenberg, Rev. Obstet. Gynecol. **2**, 212 (2009)
[2] M.H. Mosallanejad, A. Abdi, F. Karpasand, N. Nassiri, L. Iuliano, A. Saboori, Adv. Eng. Mater. **25**, 2301122 (2023)
[3] J. Grischke, J. Eberhard, M. Stiesch, Dent. Mater. J. **35**, 545 (2016)
[4] M. Kaur, K. Singh, Mater. Sci. Eng. C **102**, 844 (2019)
[5] M. Taghian, M.H. Mosallanejad, E. Lannunziata, G. Del Greco, L. Iuliano, A. Saboori, J. Mater. Res. Technol. **27**, 6484 (2023)
[6] R. Ghanavati, H. Naffakh-Moosavy, J. Mater. Res. Technol. **13**, 1628 (2021)
[7] V. Dehnavi, J.D. Henderson, C. Dharmendra, B.S. Amirkhiz, D.W. Shoesmith, J.J. Noël, M. Mohammadi, J. Electrochem. Soc. **167**, 131505 (2020)
[8] I. Aiza, C. Baldi, F.M. de la Vega, S. Sebastiani, N.E. Veronese, M. Yousefi, M.H. Mosallanejad, E. Maleki, M. Guagliano, L. Iuliano, A. Saboori, S. Bagherifard, Prog. Mater. Sci. **147**, 101357 (2025)
[9] T. DebRoy, H.L. Wei, J.S. Zuback, T. Mukherjee, J.W. Elmer, J.O. Milewski, A.M. Beese, A. Wilson-Heid, A. De, W. Zhang, Prog. Mater. Sci. **92**, 112 (2018)
[10] D. Herzog, V. Seyda, E. Wycisk, C. Emmelmann, Acta Mater. (2016).
[11] M.H. Mosallanejad, R. Ghanavati, A. Behjat, M. Taghian, A. Saboori, L. Iuliano, Metals (Basel). **14**, 425 (2024)
[12] E. Davoodi, H. Montazerian, A.S. Mirhakimi, M. Zhianmanesh, O. Ibhadode, S.I. Shahabad, R. Esmaeilizadeh, E. Sarikhani, S. Toorandaz, S.A. Sarabi, R. Nasiri, Y. Zhu, J. Kadkhodapour, B. Li, A. Khademhosseini, E. Toyserkani, Bioact. Mater. **15**, 214 (2022)
[13] L. Zhang, L. Chen, Adv. Eng. Mater. **21**, 1801215 (2019)
[14] M. Gasik, Sci. Technol. Adv. Mater. **18**, 550 (2017)
[15] T. Hanawa, Sci. Technol. Adv. Mater. **23**, 457 (2022)
[16] M. Prestat, D. Thierry, Acta Biomater. **136**, 72 (2021)
[17] J. Yang, Y. Song, K. Dong, E.H. Han, Corros. Rev. **41**, 5 (2023)
[18] N. Eliaz, Materials (Basel). **12**, 407 (2019)
[19] L. Yu, J.L. Zhu, L. Zhang, S.X. Liang, J. Cheng, L.Y. Chen, Adv. Eng. Mater. **25**, (2023).
[20] A. Bordbar-Khiabani, M. Gasik, Sci. Rep. **13**, 2312 (2023)
[21] A. Sotniczuk, J.L. Gilbert, Y. Liu, M. Matczuk, W. Chromiński, D. Kalita, M. Pisarek, H. Garbacz, Corros. Sci. **220**, 111271 (2023)

[22] E. Zhang, X. Zhao, J. Hu, R. Wang, S. Fu, G. Qin, Bioact. Mater. **6**, 2569 (2021)
[23] A. Behjat, S. Sanaei, M.H. Mosallanejad, M. Atapour, M. Sheikholeslam, A. Saboori, L. Iuliano, Biomater. Adv. **163**, 213928 (2024)
[24] P. Mahmoudi, M.R. Akbarpour, H.B. Lakeh, F. Jing, M.R. Hadidi, B. Akhavan, Mater. Today Bio. **17**, 100447 (2022)
[25] M.H. Mosallanejad, B. Niroumand, A. Aversa, A. Saboori, J. Alloy. Compd. **872**, 159567 (2021)
[26] A. Behjat, M. Shamanian, L. Iuliano, A. Saboori, Prog. Addit. Manuf. **9**, 2031 (2024)
[27] X. Xu, Y. Lu, S. Li, S. Guo, M. He, K. Luo, J. Lin, Mater. Sci. Eng. C **90**, 198 (2018)
[28] W. Zong, S. Zhang, C. Zhang, L. Ren, Q. Wang, Mater. Corros. **71**, 1697 (2020)
[29] M.H. Mosallanejad, B. Niroumand, C. Ghibaudo, S. Biamino, A. Salmi, P. Fino, A. Saboori, Addit. Manuf. **56**, 102878 (2022)
[30] A. Bordbar-Khiabani, M. Gasik, J. Mater. Res. Technol. **26**, 356 (2023)
[31] L.O. Berbel, P. Banczek, I. K. Karousis, G. A. Kotsakis, I. Costa, PLoS One **14**, (2019).
[32] F. Yu, O. Addison, A.J. Davenport, Acta Biomater. **26**, 355 (2015)
[33] L. Benea, I. Bounegru, A. Forray, E.R. Axente, D.L. Buruiana, Molecules **28**, 4837 (2023)
[34] A.C. Lazanas, M.I. Prodromidis, ACS Meas Sci. Au **3**, 162 (2023)
[35] D.S. Vieira, P.R.G. Fernandes, H. Mukai, R.S. Zola, G.G. Lenzi, E.K. Lenzi, Int. J. Electrochem. Sci. **11**, 7775 (2016)
[36] G.J. Brug, A.L.G. van den Eeden, M. Sluyters-Rehbach, J.H. Sluyters, J. Electroanal. Chem. Interfacial Electrochem. **176**, 275 (1984)
[37] S. Ren, C. Du, Z. Liu, X. Li, J. Xiong, S. Li, Appl. Surf. Sci. **506**, 144759 (2020)
[38] J. Li, D. Zhang, X. Chen, D. Xu, D. Qiu, F. Wang, M. Easton, J. Mater. Sci. Technol. **166**, 21 (2023)
[39] P. Qin, Y. Chen, Y.J. Liu, J. Zhang, L.Y. Chen, Y. Li, X. Zhang, C. Cao, H. Sun, L.C. Zhang, ACS Biomater. Sci. Eng. **5**, 1141 (2019)
[40] S. Li, H. Liu, M.A. Siddiqui, Y. Li, H. Wang, S.Y. Zhang, L. Ren, K. Yang, ACS Biomater. Sci. Eng. **9**, 2362 (2023)
[41] H. Zheng, X. Gai, Y. Bai, W. Hou, S. Li, Y. Hao, R.D.K. Misra, R. Yang, Acta Metall. Sin.-Engl. Lett. **37**, 159 (2024)
[42] X. Luo, C. Yang, D. Li, L.C. Zhang, Acta Metall. Sin.-Engl. Lett. **37**, 17 (2024)
[43] Y.W. Cui, L.Y. Chen, P. Qin, R. Li, Q. Zang, J. Peng, L. Zhang, S. Lu, L. Wang, L.C. Zhang, Corros. Sci. **203**, 110333 (2022)
[44] Y. Zhang, O. Addison, F. Yu, B.C.R. Troconis, J.R. Scully, A.J. Davenport, Sci. Rep. **8**, 3185 (2018)
[45] M.A. Siddiqui, L. Ren, D.D. Macdonald, K. Yang, Electrochim. Acta **386**, 138466 (2021)
[46] X. Gai, Y. Bai, J. Li, S. Li, W. Hou, Y. Hao, X. Zhang, R. Yang, R.D.K. Misra, Corros. Sci. **145**, 80 (2018)
[47] Y.H. Chu, L.Y. Chen, B.Y. Qin, W. Gao, F. Shang, H.Y. Yang, L. Zhang, P. Qin, L.C. Zhang, Acta Metall. Sin.-Engl. Lett. **37**, 102 (2024)
[48] H. Liu, Z.X. Wang, J. Cheng, N. Li, S.X. Liang, L. Zhang, F. Shang, D. Oleksandr, L.Y. Chen, J. Mater. Res. Technol. **27**, 7882 (2023)
[49] A. Sotniczuk, D. Kuczyńska-Zemła, P. Kwaśniak, M. Thomas, H. Garbacz, Electrochim. Acta **312**, 369 (2019)
[50] M.A. Siddiqui, I. Ullah, S.K. Kolawole, C. Peng, J. Wang, L. Ren, K. Yang, D.D. Macdonald, Corros. Sci. **190**, 109693 (2021)